$$= \lim_{\delta\to\infty} \frac{\mu I}{2\pi} \int_{D=2d+a}^{\delta} \times \left\{ 1 - \ln[2D] - \frac{\sqrt{D^2+\ell^2}}{D} + \ln\left[D + \sqrt{D^2+\ell^2}\right] \right\} dD$$

$$= \lim_{\delta\to\infty} \frac{\mu I}{2\pi} \ell \left\{ \begin{array}{l} \ln\left[\frac{\ell}{D} + \sqrt{1+\left(\frac{\ell}{D}\right)^2}\right] \\ \quad + \frac{D}{\ell} \ln\left[1 + \sqrt{1+\left(\frac{\ell}{D}\right)^2}\right] \\ +2\frac{D}{\ell}\left[1 - \sqrt{1+\left(\frac{\ell}{D}\right)^2}\right] - \frac{D}{\ell}\ln 2 \end{array} \right\}_{D=2d+a}^{\delta}$$

from which we derive (8).

Appendix B
Details of Derivation of (10)

We use approximate expressions 602.1 from Dwight [14] and (16) from Paul (see [5, p. 369]), respectively,

$$\ln\left[\frac{m}{n} + \sqrt{\left(\frac{m}{n}\right)^2 + 1}\right] = \ln\frac{2m}{n} + \frac{1}{4}\left(\frac{n}{m}\right)^2 - \frac{3}{32}\left(\frac{n}{m}\right)^4 + \cdots, \qquad \frac{m}{n} > 1$$

$$= \frac{m}{n} - \frac{1}{6}\left(\frac{m}{n}\right)^3 + \frac{3}{40}\left(\frac{m}{n}\right)^5 - \cdots, \qquad \frac{m}{n} < 1$$

$$\sqrt{1+\left(\frac{n}{m}\right)^2} = 1 + \frac{1}{2}\left(\frac{n}{m}\right)^2 - \frac{1}{8}\left(\frac{n}{m}\right)^4 + \frac{1}{16}\left(\frac{n}{m}\right)^6 - \cdots, \qquad \frac{n}{m} \le 1$$

$$= \frac{n}{m} + \frac{1}{2}\frac{m}{n} - \frac{1}{8}\left(\frac{m}{n}\right)^3 + \frac{1}{16}\left(\frac{m}{n}\right)^5 - \cdots, \qquad \frac{n}{m} \ge 1$$

in (9), obtaining

$$L = \frac{\mu}{2\pi}\ell \times \left\{ \begin{array}{l} \left[\ln\frac{2\ell}{a} + \frac{1}{4}\left(\frac{a}{\ell}\right)^2 - \cdots\right] - \left[1 + \frac{1}{2}\left(\frac{a}{\ell}\right)^2 - \cdots\right] + \frac{a}{\ell} \\ -\frac{H}{\ell}\left\{\left[\frac{H}{\ell} - \frac{1}{6}\left(\frac{H}{\ell}\right)^3 + \cdots\right] - \left[\frac{\ell}{H} + \frac{1}{2}\frac{H}{\ell} - \cdots\right] \right. \\ \qquad \left. - \ln\frac{2H}{\ell} + 1\right\} \end{array} \right\}$$

from which we derive (10).

References

[1] F. M. Tesche, M. Ianoz, and T. Karlsson, *EMC Analysis Methods and Computational Models*. New York: Wiley, 1997.

[2] E. D. Sunde, *Earth Conduction Effects in Transmission Systems*, 2nd ed. New York: Dover, 1968.

[3] L. Grcev, "Modeling of grounding electrodes under lightning currents," *IEEE Trans. Electromagn. Compat.*, vol. 51, no. 3, pp. 559–571, Aug. 2009.

[4] L. Grcev and S. Grceva, "On HF circuit models of horizontal grounding electrodes," *IEEE Trans. Electromagn. Compat.*, vol. 51, no. 3, pp. 873–875, Aug. 2009.

[5] C. R. Paul, *Inductance: Loop and Partial*. New York: Wiley-IEEE, 2010.

[6] E. B. Rosa, "The self and mutual inductances of linear conductors," *Bull. Bur. Standards*, vol. 4, no. 2, pp. 301–344, 1908.

[7] A. Banos and J. P. Wesley. (1953, Sep.). The horizontal electric dipole in a conducting half-space. Scripps Inst. Oceanogr., Marine Phys. Lab., Univ. Cal., Rep. 53-33, ch. 4 [Online]. Available: http://repositories.cdlib.org/sio/reference/53-33

[8] A. Sommerfeld, *Partial Differential Equations in Physics*. New York: Academic, 1949.

[9] A. Banos, *Dipole Radiation in the Presence of a Conducting Half-Space*. New York: Pergamon, 1966.

[10] M. B. Kraichman, *Handbook of Electromagnetic Propagation in Conducting Media*. Washington, DC: Headquarters Naval Material Command, NAVMAT P-2302, U.S. Govt. Printing Office, 2nd Printing, 1976.

[11] D. L. Jones and C. P. Burke, "The DC field components of horizontal and vertical electric dipole sources immersed in three-layered stratified media," *Ann. Geophysicae*, vol. 15, no. 4, pp. 503–510, 1997.

[12] J. R. Wait, "The false image of a line current within a conducting halfspace," *IEEE Trans. Electromagn. Compat.*, vol. 39, no. 3, pp. 266–267, Aug. 1997.

[13] C. R. Paul, *Introduction to Electromagnetic Compatibility*. New York: Wiley, 1992.

[14] H. B. Dwight, *Tables of Integrals and Other Mathematical Data*, 4th ed. New York: Macmillan, 1961.

[15] Yaqing Liu, N. Theethayi, and R. Thottappillil, "An engineering model for transient analysis of grounding system under lightning strikes: Nonuniform transmission-line approach," *IEEE Trans. Power Del.*, vol. 20, no. 2, pp. 722–730, Apr. 2005.

Improvements to a Method for Estimating the Maximum Radiated Emissions From PCBs With Cables

Changyi Su and Todd H. Hubing

***Abstract*—It has been shown in previous studies that the coupling from ICs, traces, or heatsinks on a printed circuit board to an attached cable can be modeled by placing equivalent common-mode sources between the board and the cable. In a 2008 paper published in the IEEE TRANSACTIONS ON ELECTROMAGNETIC COMPATIBILITY, a closed-form expression was developed to estimate the maximum radiated emissions from board-source-cable structures. While this expression is reasonably accurate for frequencies not exceeding 500 MHz, it may unnecessarily overestimate the emissions in some situations, especially when the maximum frequency of interest is extended beyond 500 MHz. This paper introduces two enhancements to the previously introduced closed-form expression based on improved methods for determining the maximum value of $F(\theta,k,l_{\mathrm{ant}})$ and the effective board size. The new closed-form expression is evaluated for various board geometries and frequency ranges by comparing the estimated maximum radiated emissions to full-wave simulation results.**

***Index Terms*—Common mode, electromagnetic modeling, electromagnetic radiation, imbalance difference model.**

Manuscript received May 15, 2011; revised July 9, 2011; accepted August 8, 2011. Date of publication September 26, 2011; date of current version November 18, 2011. This work was supported in part by the National Science Foundation I/UCRC for Electromagnetic Compatibility.

The authors are with Clemson University, Clemson, SC 29634 USA (e-mail: csu@clemson.edu; hubing@clemson.edu).

Color versions of one or more of the figures in this paper are available online at http://ieeexplore.ieee.org.

Digital Object Identifier 10.1109/TEMC.2011.2165217

I. Introduction

Previous studies have shown that the coupling from integrated circuits (ICs), traces, or heatsinks on a printed circuit board to attached cables can be effectively modeled by placing equivalent voltage sources between the cables and the board [2]–[5]. The maximum radiated emissions due to the common-mode current on the cable can be estimated using a closed-form equation based on the board-equivalent-source-cable geometry [1]. The closed-form expression in [1] has been shown to be reasonably accurate for various board and cable geometries. The agreement between the estimates and full-wave simulation results was shown to be within a few decibels at frequencies up to 500 MHz.

While this is good accuracy for a closed-form estimate, this paper presents two modifications to the original estimation method that extend the frequency range and improve the accuracy of the estimate. In [1], the maximum radiated emissions were calculated using a constant, maximum value for a quantity called $F(\theta,k,l_{\rm ant})$ associated with monopole radiation. This function is expressed as

$$F\left(\theta,k,l_{\rm ant}\right)=\left|\frac{\cos\left(kl_{\rm ant}\cos\theta\right)-\cos\left(kl_{\rm ant}\right)}{\sin\theta}\right| \tag{1}$$

where k is the wavenumber ($k=2\pi/\lambda$), θ is a variable between 0 and $\pi/2$, and $l_{\rm ant}$ is the monopole height above ground.

Since the envelope of $F(\theta,k,l_{\rm ant})$ is a monotonically increasing function of frequency, this method overestimates emission levels at low frequencies, especially at the first resonance. The overestimation is worse when constant values of $F(\theta,k,l_{\rm ant})$ are applied to frequency ranges extending beyond 500 MHz. Also, it was shown in [1] that maximum current is achieved when the board-source-cable geometry is approximately a quarter wavelength long. A board factor was introduced to account for the limiting effect that the board size has on the maximum field at low frequencies. The board factor is a sinusoidal function of the effective length of the board. In [1], the diagonal length of the board is used as the effective length for both rectangular and square boards. However, it is more accurate to use an approximation that more accurately accounts for the shape of the board.

II. Envelope of $F(\theta,k,l_{\rm ant})$

In [1], the closed-form expression for estimating the maximum radiation, 3 m from the source, is given by

$$|E|_{\max}=20\times\frac{1}{37}\times 2.76\times\text{board\_factor}\times\text{cable\_factor} \tag{2a}$$

where

$$\text{board\_factor}=\begin{cases}\sin\left(2\pi l_{\rm board}/\lambda\right) & \text{when } l_{\rm board}\le\dfrac{\lambda}{4}\\ 1.0, & \text{otherwise}\end{cases} \tag{2b}$$

$$\text{cable\_factor}=\begin{cases}\sin\left(2\pi l_{\rm cable}/\lambda\right) & \text{when } l_{\rm cable}\le\dfrac{\lambda}{4}\\ 1.0, & \text{otherwise}\end{cases} \tag{2c}$$

and

$$l_{\rm board}=\sqrt{L^2+W^2} \tag{2d}$$

with L and W denoting the board length and width, respectively.

In this expression, the value 2.76 represents the maximum value of $F(\theta,k,l_{\rm ant})$ in (1) when the maximum frequency of interest is 500 MHz. However, the maximum value of $F(\theta,k,l_{\rm ant})$ is not constant and increases on average with frequency. Hence, using a constant value of 2.76 tends to overestimate the values of E at frequencies well below 500 MHz and may underestimate the values of E when applied to frequencies above 500 MHz.

The maximum values of $F(\theta,k,l_{\rm ant})$ are obtained when

$$kl_{\rm ant}=n\pi, n=1,2,... \tag{3}$$

Combining (3) and (1), the maximum values of $F(\theta,k,l_{\rm ant})$ are

$$\begin{aligned}F_{\max}\left(\theta,n\right)&=\left|\frac{\cos\left(n\pi\cos\theta\right)-\cos\left(n\pi\right)}{\sin\theta}\right|\\&=\left|\frac{\cos\left(n\pi\cos\theta\right)-(-1)^n}{\sin\theta}\right|.\end{aligned} \tag{4}$$

The cos(θ) terms can be approximated by the first two terms of their Taylor's polynomials

$$\cos\theta\approx 1-\frac{\theta^2}{2},\quad\text{when } |\theta|<\frac{\pi}{2}. \tag{5}$$

This results in a simplified version of (4):

$$F_{\max}\left(\theta,n\right)\approx\left|\frac{1-\cos\left(\dfrac{n\pi\theta^2}{2}\right)}{\sin\theta}\right|. \tag{6}$$

The maximum values of (6) are achieved when $\cos(\frac{n\pi\theta^2}{2})=-1$, or

$$\theta=\sqrt{\frac{2}{n}}. \tag{7}$$

Combining (6) and (7), we have

$$F_{\max}\left(n\right)\approx\left|\frac{2}{\sin\sqrt{\dfrac{2}{n}}}\right|,\quad n=1,\,2,\,... \tag{8}$$

To get a continuous function that captures all the peaks, the discrete function in (8) is replaced by its continuous envelope by substituting α for n

$$F_{\max}\left(\alpha\right)\approx\left|\frac{2}{\sin\left(\sqrt{\dfrac{2}{\alpha}}\right)}\right| \tag{9}$$

where α ($\ge$1) is a real continuous variable function of frequency and is given by

$$\alpha=\frac{2fl_{\rm ant}}{c_0} \tag{10}$$

where c_0 is the speed of light in free space.

Since $\alpha\ge$1, the value of (9) is always positive. The maximum value at $\alpha=1$ is used for all frequencies corresponding to $\alpha<1$.

Combining (9) and (10), we have

$$F_{\max}\left(f\right)\simeq\begin{cases}\dfrac{2}{\sin\sqrt{2}} & f\le\dfrac{c_0}{2l_{\rm ant}}\\ \dfrac{2}{\sin\left(\sqrt{\dfrac{c_0}{fl_{\rm ant}}}\right)} & f>\dfrac{c_0}{2l_{\rm ant}}.\end{cases} \tag{11}$$

Fig. 1 shows the envelope of $F(\theta,k,l_{\rm ant})$ between 0 and 1 GHz. In this plot, $F_{\max}$ is obtained from (4) using $\theta=\sqrt{2/\alpha}$ with $\alpha=2fl_{\rm ant}/c_0$. The dashed line represents the maximum value of $F(\theta,k,l_{\rm ant})$ over the entire frequency range. Instead of using the maximum value over the

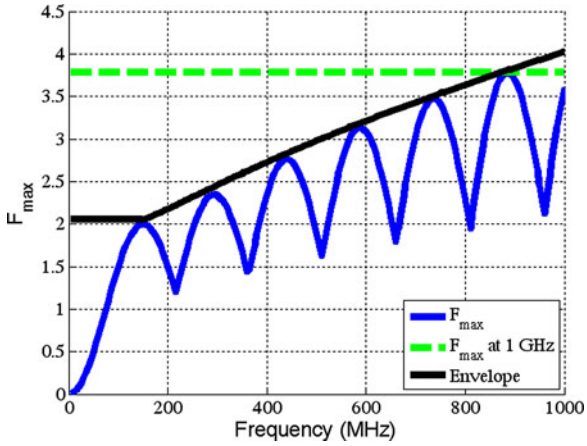

Fig. 1. Maximum values of $F(\theta,k,l_{\text{ant}})$.

entire range, the envelope [obtained by (11)] shown by the solid black line gives the exact maximum value at each resonance. The tendency to overestimate at the lower frequencies is eliminated and the accuracy is improved.

By replacing the constant 2.76 in (1) with (11), the new closed-form estimate for the maximum radiation can be written as

$$|E|_{\max} \simeq \begin{cases} 20 \times \dfrac{1}{37} \times \dfrac{2}{\sin\left(\sqrt{2}\right)} \times \text{bfac} \times \text{cfac} & f \le \dfrac{c_0}{2l_{\text{ant}}} \\ 20 \times \dfrac{1}{37} \times \dfrac{2}{\sin\left(\sqrt{\dfrac{c_0}{f l_{\text{ant}}}}\right)} \times \text{bfac} \times \text{cfac} & f > \dfrac{c_0}{2l_{\text{ant}}} \end{cases} \tag{12}$$

where bfac and cfac are the board_factor and cable_factor, respectively.

III. Improved Expression for Calculating the Effective Board Length

In [1], the effective length of a rectangular board is set equal to the diagonal length. This is a good approximation when the ratio of the board length to width is large. However, a broader board tends to present a lower impedance. In other words, a nearly square board has a longer effective length than a narrow board with the same diagonal length. An empirical equation for approximating the length can be found in [7]:

$$l_{\text{eff,board}} = \frac{\sqrt{L^2 + W^2}}{A} \tag{13}$$

where A is a function of the board dimensions given by

$$A = \frac{L/2a}{1 + L/2a}, \quad a = \frac{W}{4}. \tag{14}$$

Combining (13) and (14), we have

$$l_{\text{eff,board}} = \frac{1 + 2L/W}{2L/W} \times \sqrt{L^2 + W^2}. \tag{15}$$

When the board is very narrow, the effective length is roughly equal to the diagonal length. As the board width increases, the effective length becomes larger than the diagonal length. Substituting $l_{\text{eff,board}}$ in (15) for l_{board} in (2b), an improved closed-form expression for the

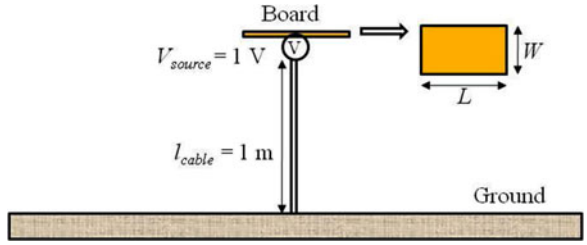

Fig. 2. Geometry used to validate the new estimate.

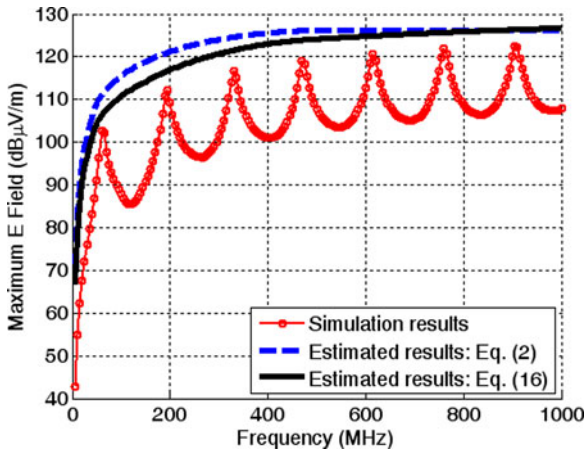

Fig. 3. Maximum radiation for a 14-cm × 2-cm rectangular board.

maximum radiated emissions is obtained:

$$|E|_{\max} \simeq \begin{cases} 20 \times \dfrac{1}{37} \times \dfrac{2}{\sin\left(\sqrt{2}\right)} \times \text{bfac} \times \text{cfac} & f \le \dfrac{c_0}{2l_{\text{ant}}} \\ 20 \times \dfrac{1}{37} \times \dfrac{2}{\sin\left(\sqrt{\dfrac{c_0}{f l_{\text{ant}}}}\right)} \times \text{bfac} \times \text{cfac} & f > \dfrac{c_0}{2l_{\text{ant}}} \end{cases} \tag{16a}$$

where

$$\text{bfac} = \begin{cases} \sin\left(2\pi l_{\text{eff,board}}/\lambda\right) & \text{when } l_{\text{eff,board}} \le \dfrac{\lambda}{4} \\ 1.0, & \text{otherwise} \end{cases} \tag{16b}$$

$$\text{cfac} = \begin{cases} \sin\left(2\pi l_{\text{cable}}/\lambda\right) & \text{when } l_{\text{cable}} \le \dfrac{\lambda}{4} \\ 1.0, & \text{otherwise} \end{cases} \tag{16c}$$

and

$$l_{\text{eff,board}} = \frac{1 + 2L/W}{2L/W} \times \sqrt{L^2 + W^2}. \tag{16d}$$

IV. Validation

To validate the new estimate, the test configurations evaluated in [1] are reevaluated over wider bandwidths. Fig. 2 shows the simplified structure of a board with an attached cable, where a 1-V source is connected to the center of the board. It was demonstrated in [1] that the peak emissions are relatively independent of the connection point to the board. The cable is 1 m long and attached to an infinite ground plane at its base.

The estimates in (2) and (16) are compared to full-wave simulation results [6]. Fig. 3 shows a plot of closed-form estimates and simulation results for a 14-cm × 2-cm rectangular board at frequencies up to

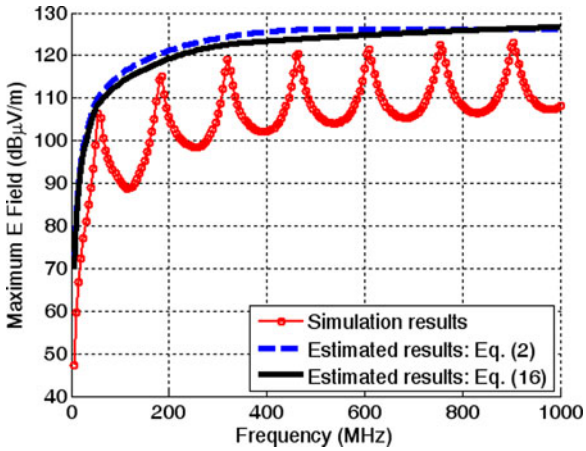

Fig. 4. Maximum radiation for a 10-cm square board.

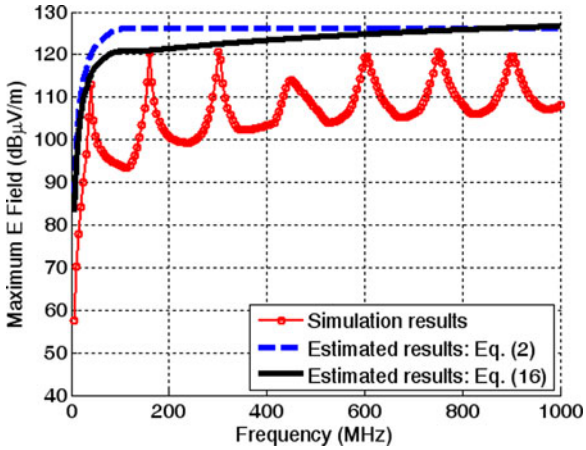

Fig. 5. Maximum radiation for a 63-cm × 9-cm rectangular board.

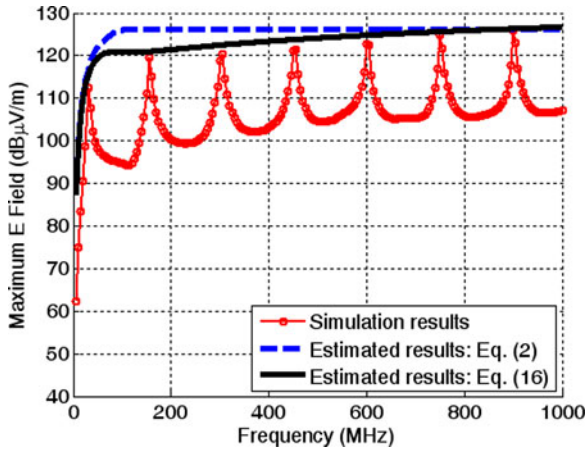

Fig. 6. Maximum radiation for a 45-cm square board.

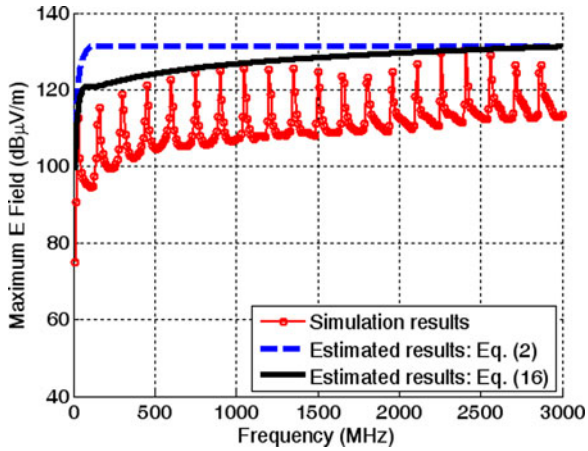

Fig. 7. Maximum radiation for a 45-cm square board up to 3 GHz.

1 GHz. Using (2) with a value of 3.66 substituted for the 2.76 to account for the wider bandwidth, the peak emissions at low frequencies are over predicted. The value 3.66 is the maximum value of $F(\theta,k,l_{\mathrm{ant}})$ for frequencies up to 1 GHz. The estimate using (16) eliminates the overestimation at low frequencies and the accuracy is comparable to (2) at high frequencies. Fig. 4 illustrates a similar plot for a 10-cm square board. The estimates are different for square and rectangular boards that have the same diagonal length. The effective length of a square board is slightly longer than that of a rectangular board, and consequently, the resonant frequencies of the square board are slightly shifted to the left. By using the new effective length in (15), the board factor in (16) accounts for the frequency shift at low frequencies. The maximum radiation for a 63-cm × 9-cm rectangular board and a 45-cm square board are plotted in Figs. 5 and 6, respectively. The closed-form expression in (16) does a reasonable job of estimating the maximum emissions for both of these large board dimensions.

The improvement in the accuracy of the estimate is even greater when the maximum frequency is further extended. To illustrate this, the configuration in Fig. 6 was evaluated between 10 MHz and 3 GHz, as shown in Fig. 7. For the results shown, a new constant, 6.78, replaced the 2.76 term in (2). The value 6.78 is the maximum value of $F(\theta,k,l_{\mathrm{ant}})$ for frequencies up to 3 GHz. Note that this causes the lower frequency peaks to be significantly overestimated. The new estimate improves the accuracy at low frequencies by up to 10 dB.

V. Conclusion

This paper describes two improvements to the method introduced in [1]. The accuracy of the estimate at low frequencies and for larger frequency ranges is improved by using an expression for the envelope of $F(\theta,k,l_{\mathrm{ant}})$ that equals the maximum value at every resonant frequency. A modified expression for calculating the effective length of the board improves the accuracy of the estimate when applied to nearly square boards.

References

[1] S. Deng, T. Hubing, and D. Beetner, "Estimating maximum radiated emissions from printed circuit boards with an attached cable," *IEEE Trans. Electromagn. Compat.*, vol. 50, no. 1, pp. 215–218, Feb. 2008.

[2] D. M. Hockanson, J. L. Drewniak, T. H. Hubing, T. P. Van Doren, F. Sha, and M. Wilhelm, "Investigation of fundamental EMI source mechanisms driving common-mode radiation from printed circuit boards with attached cables," *IEEE Trans. Electromagn. Compat.*, vol. 38, no. 4, pp. 557–566, Nov. 1996.

[3] W. Cui, H. Shi, X. Luo, J. L. Drewniak, T. P. Van Doren, and T. Anderson, "Lumped-element sections for modeling coupling between high-speed digital and I/O lines," in *Proc. IEEE Int. Symp. Electromagn. Compat.*, Austin, TX, Aug.1997, pp. 260–265.

[4] N. Oka, C. Miyazaki, and S. Nitta, "Radiation from a PCB with coupling between a low frequency and a digital signal traces," in *Proc. IEEE Int. Symp. Electromagn. Compat.*, Aug. 1998, pp. 635–640.

[5] H. Shim and T. Hubing, "Model for estimating radiated emissions from a printed circuit Board with attached cables driven by voltage-driven sources," *IEEE Trans. Electromagn. Compat.*, vol. 47, no. 4, pp. 899–907, Nov. 2005.
[6] *FEKO User's Manual, Suite 6.0*, EM Softw. Syst. (S.A.) (Pty), Ltd., Stellenbosch, South Africa, Sep. 2010, 2011.
[7] J. D. Kraus, *Antennas*. New York: McGraw-Hill, 1950, pp. 276–278.

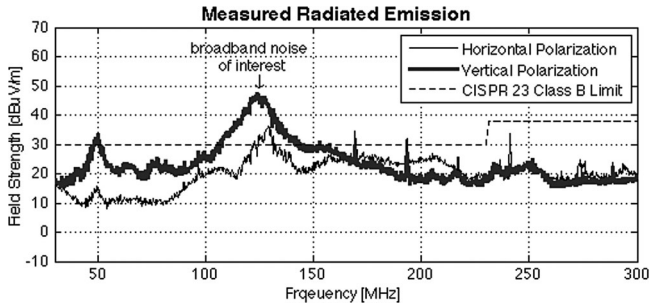

Fig. 1. Measured radiated emissions.

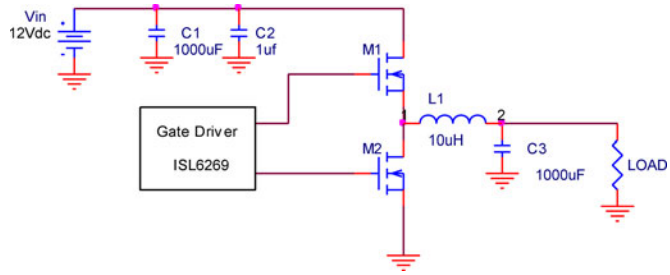

Fig. 2. Synchronous buck converter.

Quantification of Self-Damping of Power MOSFET in a Synchronous Buck Converter

Keong Kam, David Pommerenke, Ankit Bhargava, Bob Steinfeld, Cheung-wei Lam, and Federico Centola

***Abstract*—Ringing in the switching waveform of the switching power supply (e.g., synchronous buck converter) is known to cause broadband electromagnetic interference problems in the 30–300 MHz range. The measured switching waveform shows overshoot and, then, exponential decay of the ringing. It has been observed that this exponential decay rate varies significantly between using different low-side FETs; thus, the low-side FET dominates the attenuation of the ringing. This paper provides a novel method for quantifying the losses by using the measureable quantity "R_{oss}," which is equivalent to the loss of the output capacitance C_{oss} of the FET. This paper describes the method of measuring R_{oss} and explains its relevance to the self-damping of the switch ringing. The method permits selection of a low-side FET to optimize the electromagnetic compatibility performances of the supply.**

***Index Terms*—Buck converter electromagnetic interference (EMI), FET device parameter R_{oss}, broadband EMI, switch ringing.**

I. Introduction

Switching power supplies are widely being used in today's electronic systems because of their high efficiency; however, they often cause electromagnetic interference (EMI) issues because of their nature of high *dv/dt* and *di/dt* [1]. A synchronous buck converter is one of the most popular switching power supply topologies used for stepping voltage down. The switching waveform for this type of converter often exhibits ringing due to the parasitic *LC* resonance in the switching loop [2]. This ringing is known to cause broadband EMI problems, the frequency of which is centered at the ringing frequency. Fig. 1 shows an example of the broadband noise observed in the measured radiated emissions from a prototype computer system. The broadband emission is shown around 125 MHz.

Much of recent effort has been focused on solving broadband EMI issues related to the synchronous buck converter. Researchers have proposed several approaches, including addition of circuit elements (e.g., passive/active snubber, input filtering) and layout optimization [3].

It was observed that the selection of FETs greatly affects the switching waveform, in general, and the ringing frequency and its attenuation specifically. Many parameters contribute to the switching waveform; these include capacitances (gate capacitance, output capacitance), driver strength, and body-diode reverse-recovery characteristics, and different parameters influence different aspects of the switching waveform (e.g., rise time, overshoot, ringing frequency, and decay rate). This paper concentrates on one parameter, i.e., R_{oss}, which has a dominant effect on the damping of the ringing. R_{oss} has been previously introduced by [4] in an analysis of the losses of very high frequency dc/dc converters.

In Section II, we demonstrate the significance of FET selection with respect to switching waveform ringing and the corresponding effects on EMI. In Section III, we present quantification of the loss related to the switch ringing attenuation. In Section IV, we show that the missing piece of the loss mechanism is R_{oss} of the low-side FET.

II. Effect of FET Selection in Switch Ringing

Fig. 2 shows a typical schematic of a synchronous buck converter. In this topology, the two switches M1 and M2 alternate, and this switching produces lower output voltage than the input voltage.

The following experimental results show the effect of low-side FET (M2) selection on the switching waveform in a synchronous buck converter. The test board used in the measurement comprised a single synchronous buck converter operating at 12 V input and 3.3 V, 3.3 A output. The switching frequency of the converter was 300 KHz.

This measurement used the same gate driver and the high-side FET (M1). Several different FETs from various manufacturers (see Table I) served as a low-side FET. Fig. 3 shows the measured switching waveforms.

The ringing on the rising edge is of interest in this case since the ringing on the rising edge is known to be the root cause of the broadband EMI from synchronous buck converters [1]–[3].

Manuscript received August 30, 2010; revised February 14, 2011; accepted March 20, 2011. Date of publication August 15, 2011; date of current version November 18, 2011.

K. Kam, D. Pommerenke, and A. Bhargava are with the Missouri University of Science and Technology, Rolla, MO 65401 USA (e-mail: kwkx8d@mst.edu; davidjp@mst.edu; aab262@mst.edu).

B. Steinfeld, C.-w. Lam, and F. Centola are with Apple Inc., CA 95014 USA (e-mail: steinfe1@apple.com; lam@apple.com; centola@apple.com).

Color versions of one or more of the figures in this paper are available online at http://ieeexplore.ieee.org.

Digital Object Identifier 10.1109/TEMC.2011.2157165